



Optimization and simulation of pulsed electric field treatment chamber for food sterilization

Yuxuan WANG¹ , Kaiyue SHA¹, Xuyao GUO¹, Jing CHEN¹, Quanzhen CHEN¹, Feng JIANG^{1*}

Abstract

Pulsed Electric field (PEF) cell lysis technology, as a new technology, has been widely used in the fields of food sterilization. Nowadays, there are still several problems in PEF cell lysis: low cell lysis rate, high temperature rise, the presence of low velocity regions, etc. In this study, COMSOL Multiphysics was used to conduct simulation research, and the electric field, flow field and temperature field of plate treatment chamber, coaxial treatment chamber and co-field treatment chamber were coupled to simulate, and the advantages and disadvantages of the three classical treatment chamber structures were analyzed. In addition, this paper proposes a new structure of the co-field treatment chamber. Through the comparison and simulation of the coupling between our design and other four structures, the electric field intensity of our design treatment area is 20.03 kV/m, which is 46.2% higher than the highest of others. The temperature rise within 1s is 0.93 K, which is 2/3 lower than others. Our design almost eliminates the peak electric field area at the junction between the inside of the electrode and the insulator, and the maximum electric field intensity in this area is reduced by 24.4% compared with others.

Keywords: cell lysis; pulsed electric field; electroporation effect of cells; co-field treatment chamber; food sterilization.

Practical Application: Sterilization of liquid food.

1 Introduction

Food sterilization is one of the difficult problems in food engineering. Compared with the traditional sterilization technology (such as pasteurization) and high-temperature short time (HTST), which are the main food sterilization strategies, non-thermal sterilization technology will not cause damage to the nutritional value of food due to excessive heating, and has been widely concerned by the academic community. Non-thermal sterilization technology refers to the technology that sterilizes food by means other than thermal effect, including low temperature and high hydrostatic pressure (HHP) (Deng et al., 2021), pulsed electric field (PEF) (Prestes et al., 2022) and magnetic field (Abdilova et al., 2021), etc.

The main principle of pulsed electric field (PEF) treatment is to treat food by applying high field intensity of tens of thousands of volts per centimeter, pulse width of microsecond or nanosecond and extreme pulse frequency, and destroy the biofilm structure by electroporation effect (Tsong, 1989) to achieve sterilization effect. It has the advantages of fast processing speed, strong controllability and no harmful residue. In addition, Arshad et al. (2021a) pointed out in their study that the use of PEF instead of traditional food processing schemes can significantly reduce food waste and achieve sustainable development in terms of conservation, nutritional safety and food safety as well as environmental friendliness. Gentès et al. (2022) discussed the influence of PEF on various indexes in cheese making, compared it with pasteurization, and found that PEF treatment had less influence on proteins while ensuring the bactericidal effect.

Not only that, research by Rocha et al. (2022) indicates that PEF treatment can also improve the color, flavor, aroma and texture characteristics of products, thus increasing the acceptability of products. By virtue of its various advantages, PEF has been widely applied and studied in the fields of food sterilization (Arshad et al., 2021b). Šalaševičius et al. (2021) and intracellular substance extraction (Naliyadhara et al., 2022;). In addition, this technique has also become a research hotspot in the field of cancer therapy due to its potential ability to selectively shatter organelle membranes and nuclear membranes (Sowmya & Varadarajan, 2021).

Xu & Xiao (2006) in the cell model of cells found in broken simulation experiment, specific parameters of microsecond pulse electric field can be a specific role in mitochondrial membrane, induce cell apoptosis, it is more efficiency than traditional electroporation make cell necrosis, because used to induce apoptosis of one over ten of the energy needed for only cause cell death, Moreover, high voltage pulsed electric field is likely to selectively destroy malignant cells. Due to its great potential in selectively eliminating cancer cells and other harmful cells, this characteristic is of great value for further study. Zheng et al. (2021) conducted three-field coupling simulation of electric field, flow field and temperature field in the treatment chamber of the plate type continuous treatment chamber, and found that the electric field distribution in the treatment chamber was not uniform, and the structure of the treatment chamber had little

Received 15 Dec., 2022

Accepted 21 Jan., 2023

¹School of Computer and Information Engineering, Central South University of Forestry and Technology, Changsha, China

*Corresponding author: jf09mail@126.com

influence on the sterilization effect when the inlet flow rate was set to 5 cm/s in the sterilization process.

Previous studies (Zhang et al., 2016a) have pointed out that one of the most important indicators in PEF cell lysis is the magnitude of the transmembrane voltage, that is, the distribution of the electric potential in the treatment chamber and the magnitude of the electric field intensity in the treatment area are an important link to determine the rate of cell lysis, while the structure of the treatment chamber is one of the main factors to determine the distribution of electric field.

When the high voltage electric field is applied, there is always the conversion of electric potential energy to internal energy, which leads to the rise of local temperature in the treatment chamber. Although this temperature rise effect can increase the mortality of bacteria to a certain extent, it may also lead to protein denaturation and destroy the nutritional value of food itself. Moreover, if the temperature rise effect leads to bubble generation, the electrical parameters in the treatment chamber will be changed, and the electrical breakdown will be more easily triggered, which will further increase the loss of PEF cell crusher itself and the hidden danger of safety accidents. At the same time, due to the complexity of the structure of some treatment chambers, the flow rate dead zone may be generated in the work, and this low flow rate area is easy to cause further local temperature rise. Therefore, how to eliminate the low-velocity zone and reduce the temperature rise should not be ignored in the study of PEF cell lysis.

Due to the phenomenon of excessive electric field intensity at the edge of the electrode plate in the co-field treatment chamber, the local temperature is too high and the temperature rises too fast, which damages the nutritional value of food and leads to the destruction of cell contents. To solve this problem, Zhang et al. (2016b) found that slightly changing the insulator structure in the PEF treatment chamber could significantly change the intensity and uniformity of the electric field generated in the treatment chamber. The improved methods, such as reducing the inner diameter of insulator, rectifying the inner rectangle and ellipse, can greatly improve the uniformity of electric field and the flow mode of turbulent fluid. Numerical simulation results show that the temperature rise induced by electric field can be reduced by changing the insulator geometry. These characteristics will reduce the damage of high voltage pulsed electric field food sterilization to the nutritional value and taste of processed food materials, and realize the energy saving and efficient operation of high voltage pulsed electric field food sterilization equipment. The study of Zand et al. (2021) also pointed out that changes in electrical conductivity and electrode structure or area may lead to different levels of electroporation.

Therefore, this paper aims to use COMSOL Multiphysics field simulation software to study the influence of the treatment chamber structure on the electric field distribution, the flow rate and temperature rise effect in the treatment chamber during the process of cell lysis, in order to provide some ideas for the structure design of PEF cell lysis treatment chamber.

2 Theoretical basis of simulation

2.1 Electroporation effect of cells

As a structure that protects the cell body and is responsible for the exchange of materials inside and outside the cell, the

membrane is about 7-8 nm thick. Its basic composition is phospholipid bilayer as a scaffold and some glycoproteins, proteins and glycolipids. The phospholipid layer is responsible for insulating the outside world from the inside of the cell, preventing most substances from moving in and out of the cell freely; The sugar chain is responsible for the exchange of information between the cell and the outside world; Protein channels are responsible for ion exchange with the outside world and so on. This ability to allow a subset of molecules to cross the cell membrane is called selective transmissibility -- a property that keeps the cell relatively stable, allowing essential substances to enter and secretions and wastes to escape. Therefore, the selective permeability of cell membrane must be destroyed in order to extract non-secretory substances.

There are various opinions on the electrochemical causes of cell lysis in PEF, including electrical release, electrical energy conversion into mechanical energy resulting in lysis, magnetic lysis, etc. One of the widely accepted explanations in the academic field is the electroporation effect of membrane in pulsed electric field (Guo et al., 2020; Glaser et al., 1988). Therefore, in order to determine the specific direction of simulation experiment and the measurement standard of simulation results, we should fully understand the mechanism of electroporation.

As shown in Figure 1a, the normal phospholipid bilayer is tightly packed, preventing the passage of most substances; When an electric field E is applied to it, the distance between some phospholipid molecules in Figure 1b begins to increase due to the increase of the transmembrane voltage, but the pores generated at this time are still hydrophobic because the molecules have not been reorganized. When E increases to a certain degree, the radius of the drainage hole of the visible Figure 1c expanded threshold, the phospholipid molecules start restructuring, originally the drainage hole of change structure to hydrophilic at one hole, namely changes drainage hole to hole, since cells inside and outside material can freely through the cell membrane, also due to free access of the ions across the membrane voltage decreases.

At this time, the cell membrane loses its selective permeability, and electroporation is completed. According to whether it can heal or not, electroporation is divided into reversible electroporation and irreversible electroporation. Reversible electroporation is generally used in cell fusion, DNA implantation and other fields, while irreversible electroporation is generally used in intracellular material extraction, bacterial elimination and tumor treatment.

2.2 Governing equation

In this study, it is necessary to conduct the coupling simulation of electric field, flow field and temperature field for PEF treatment chambers with different structures. Therefore, when the physical quantities contained in the three fields are constrained, the equations applied are the charge conservation equation, the continuity equation of the fluid, the momentum conservation equation and the energy conservation equation.

First is the electric field governing equation (charge conservation Equation 1):

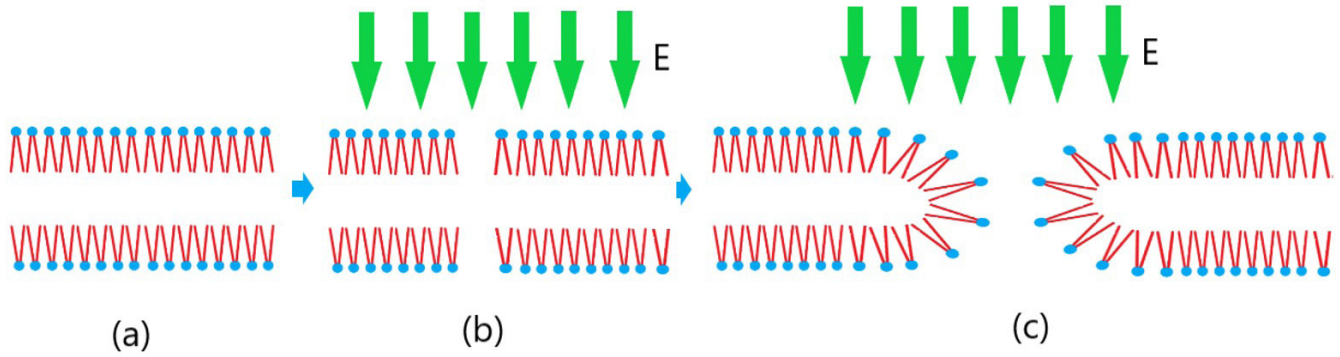


Figure 1. Electroporation of membrane.

$$\nabla \cdot \mathbf{J} = \rho_{j,v} \quad (1)$$

Where ∇ is nabla operator; \mathbf{J} is the current density, unit: A/m^2 ; $\rho_{j,v}$ is the amount of charge in C. This formula means that the curl of the current density is equal to the total charge.

Where (Equation 2),

$$\mathbf{J} = \sigma(T)\mathbf{E} + \frac{\partial \mathbf{D}}{\partial t} + \mathbf{J}_e \quad (2)$$

In equation 2, $\sigma(T)$ is the function of electrical conductivity σ as a function of temperature T , and the unit is S/m ; \mathbf{E} is electric field intensity, unit V/m ; \mathbf{D} is the electric displacement (induction intensity), the unit is C/m^2 ; \mathbf{J}_e is the current density of the transport current, expressed in A/m^2 . This formula means that the full current density is equal to the sum of the conduction current density, displacement current density and transport current density.

Assuming that the pulsed electric field does not generate a changing magnetic field, there is Equation 3:

$$\mathbf{E} = -\nabla V \quad (3)$$

V is the point potential, unit: V . That is, the electric field intensity vector and the potential divergence vector are equal and opposite.

Reynolds number is calculated using the following Equation 4:

$$Re = \frac{\rho v d}{\eta} \quad (4)$$

Where, Re is the Reynolds number of the fluid; ρ is the fluid density, unit: kg/m^3 ; v is the fluid velocity in m/s ; d is the characteristic length (fluid channel diameter), and the unit is m ; η is the dynamic viscosity of the fluid in $Pa \cdot s$.

Because when the Reynolds number Re is less than 2300, the fluid is laminar flow, when Re is between 2300 and 4000, it is a transition state, and when Re is greater than 4000, it is turbulent flow. Therefore, it can be known by calculation that the flow rate of 293 K water at one atmospheric pressure in a channel with a diameter of 8mm is turbulent when the flow rate is greater than 1.48554 m/s , and laminar flow when it is less than 0.85419 m/s . The fluid velocity used in this simulation is 55.3 mm/s corresponding to the laboratory scale of 10 L/h , so the flow type is laminar flow. Because the low-velocity zone can

be eliminated more effectively when the fluid is in the turbulent state than in the laminar state, if the turbulence intensity in the main working area can be increased by changing the structure of the treatment chamber, it will be helpful to eliminate the velocity dead zone.

Assuming that the fluids in this simulation are all Newtonian fluids, the continuity Equation 5 of the fluid is as follows:

$$\frac{\partial \rho(p, T)}{\partial t} + \nabla \cdot [\rho(p, T)\mathbf{v}] = 0 \quad (5)$$

Where, $\rho(p, T)$ represents the density ρ as a function of pressure p and temperature T , unit kg/m^3 ; t is time, unit s . This formula is derived from the mass conservation formula and is applicable to all flow fields.

The governing equation of temperature field is energy conservation Equation 6:

$$\rho(p, T)C_p(T)\left(\frac{\partial T}{\partial t} + \mathbf{v} \cdot \nabla T\right) = Q_e + \nabla \cdot [k(T) \cdot \nabla T] \quad (6)$$

Where (Equation 2),

$$Q_e = \sigma(T) \cdot E^2 \quad (7)$$

In Equation 6 and Equation 7, $C_p(T)$ is the function of atmospheric heat capacity C_p as a function of temperature T ; $k(T)$ is a function of thermal conductivity as a function of temperature. Q_e represents the heat generated by the electric field as a function of the electric field strength and temperature. The governing equation describes the conversion of electrical potential energy into internal energy subject to pressure.

The governing Equation 8 of non-isothermal flow is:

$$-\mathbf{n} \cdot \mathbf{q} = \rho C_p u_\tau \frac{T_w - T}{T^+} \quad (8)$$

Where, \mathbf{n} is the boundary normal vector; \mathbf{q} is the heat flux, in W/m^2 ; u is the velocity in m/s ; T is the temperature in K . Non-isothermal flow describe fluid flows that are not constant in temperature, as the temperature of a fluid changes, the fluid's material properties (such as density and viscosity) change accordingly.

3 Structural simulation of classical PEF treatment chambers

3.1 Structure of common treatment chambers

The PEF treatment chambers which widely used nowadays can be divided into three types according to the position of the electrode: plate treatment chamber, coaxial treatment chamber (and its variants (Zhang et al., 1995; Lubicki et al., 1995), and co-field treatment chamber (and its variants (Zhang et al., 2018; Sale & Hamilton, 1967)). The structure of the three classical treatment chambers is shown in Figure 2. The red area represents the high-voltage electrode and the green part represents the ground electrode. The section of the plate treatment chamber (Figure 2a) is generally rectangular, the high voltage electrode and the ground electrode are located on both sides of the feeding tube and parallel to each other; The section of the coaxial treatment chamber (Figure 2b) is circular, the high voltage electrode is located in the middle of the pipeline, and the outside of the pipeline is grounded. The cross section of the co-field treatment chamber (Figure 2c) is generally circular, but the high-voltage electrode and ground electrode areas are located on the outside of the pipe and separated by insulating materials. Previous studies (Qingxue & Ping, 2017) have shown that different treatment chamber structures will have a considerable impact on electric field distribution, internal fluid flow and temperature rise.

3.2 Model establishment and boundary conditions

Three dimensional models of PEF treatment chamber with different structures were established in COMSOL multi-physical

simulation software. The spacing between electrodes in the plate treatment chamber was 4 mm, the thickness of both electrodes was 1 mm, and the spacing between the left and right sides of the inner wall was 10 mm. The indoor diameter of coaxial treatment is 8 mm, the thickness of ground electrode is 1 mm, and the diameter of high voltage electrode is 2 mm. The indoor diameter of the co-field treatment chamber is 8 mm, the thickness of the two ring electrodes is 1 mm, the width is 5 mm, and the length of the channel between the two electrodes is 5 mm. In addition, a rectangular solution range is set between the plate treatment chamber and the coaxial treatment chamber, so as to observe the electric field distribution and temperature rise on the outdoor side of the treatment chamber.

The model was meshed into free tetrahedrons (Figure 3), and the solution area was divided into 17171, 13072 and 19312 tetrahedrons, respectively. The minimum element masses were 0.1189, 0.08416 and 0.121, respectively.

After the mesh generation is completed, the material and boundary conditions of each part are set as follows (specific parameters is in Table 1): The electrode material was uniformly set as copper, the insulation material was Polytetrafluoroethylene (PTFE), the surrounding solution area was set as air, the treatment chamber was set as cell suspension, the terminal voltage was set as 100V, and the initial temperature was 293.15 K.

Uniformly set the left side of each treatment chamber model as the fluid inlet (the flow rate was set as 55.3 mm/s corresponding to the laboratory scale of 10 L/h), and the right side was the outlet. Multi-physical field electromagnetic heat and

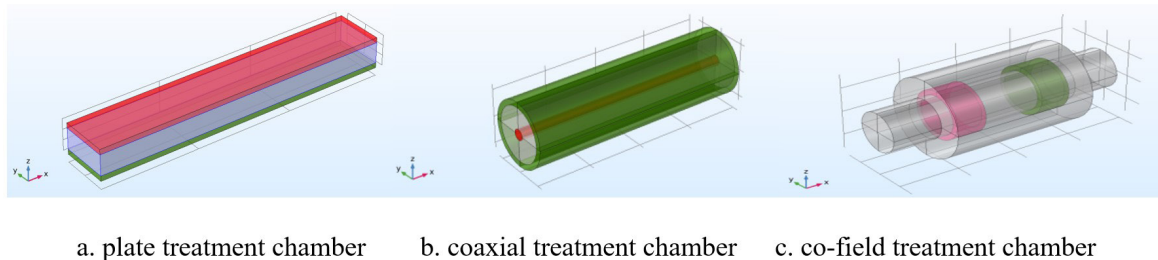


Figure 2. Structure diagram of PEF treatment chamber.

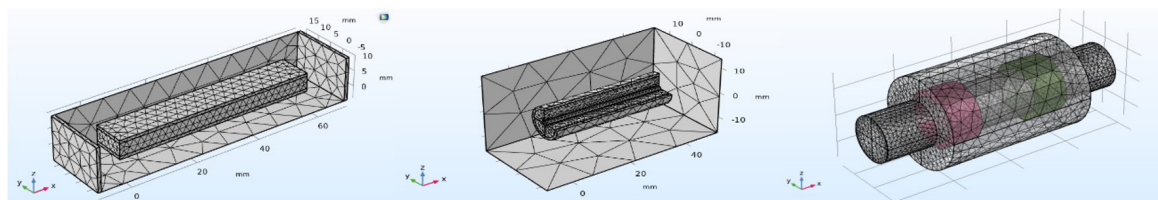


Figure 3. Mesh generation of the PEF treatment chamber (some fields have been hidden).

Table 1. parameters of each material.

material type	Relative dielectric constant	Electrical conductivity (S/m)	Density (kg/m ³)	Dynamic viscosity (Pa·s)
cell suspension	67.00	0.55	1007	1.01×10^{-3}
PTFE	2	10^{-8}	2200	-
copper	10^8	5.998×10^7	8960	-

non-isothermal flow are added simultaneously to simulate the temperature rise effect of liquid flow in the treatment chamber.

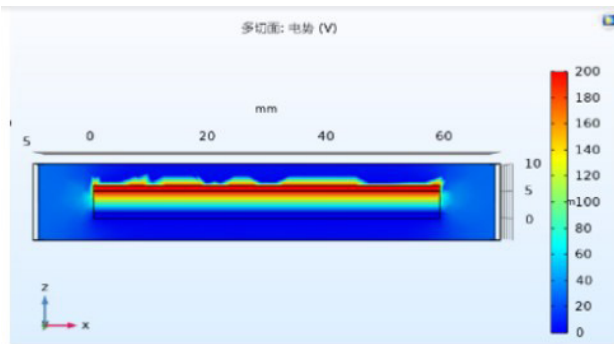
Set the study type as the transient solution from 0 to 1s with a step size of 0.1s. This simulation will analyze the simulation results of three kinds of treatment chamber structures from three main aspects: electric field distortion after stabilization, flow rate distribution and internal temperature rise rate, and discuss the advantages and disadvantages of each of them.

3.3 Experimental results

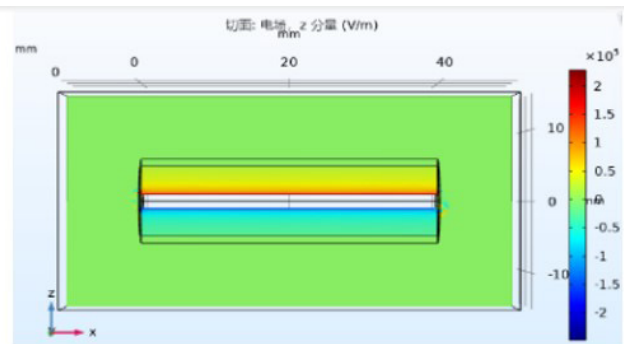
Electric field simulation results

The electric potential and electric field intensity distribution of each treatment chamber are shown in Figure 4. It can be seen from

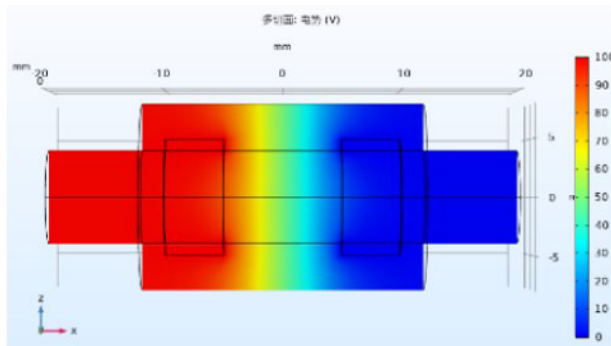
the figure that among the three treatment chambers, the electric field distribution of the plate treatment chamber (Figure 4a) is the most uniform, and the electric field distortion of the coaxial treatment chamber (Figure 4b) and the co-field treatment chamber (Figure 4c) is more serious. It can be seen from the electric field intensity distribution diagram that the electric field intensity in the plate treatment chamber is almost the same everywhere (Figure 4d), which is 50 kV/m. The electric field intensity of the coaxial treatment chamber gradually decreases outward from the high-voltage electrode at the axis (Figure 4e), ranging from 19.7 kV/m to 117.80 kV/m. The maximum electric field intensity in the co-field treatment chamber is 8.39 kV/m in the midline section of the channel (Figure 4f). In addition, under the action of strong electric field, the isopotential surface at the position with large curvature of the object surface is also dense, leading



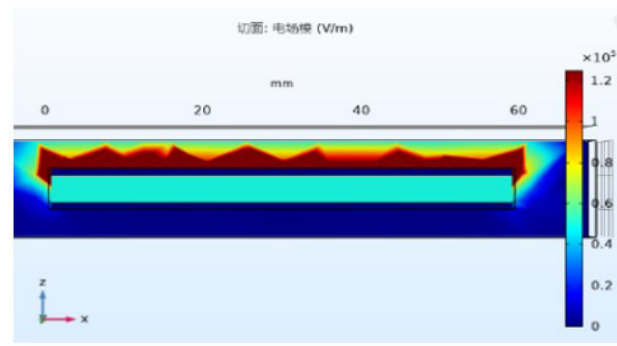
(a) electric potential of plate treatment chamber



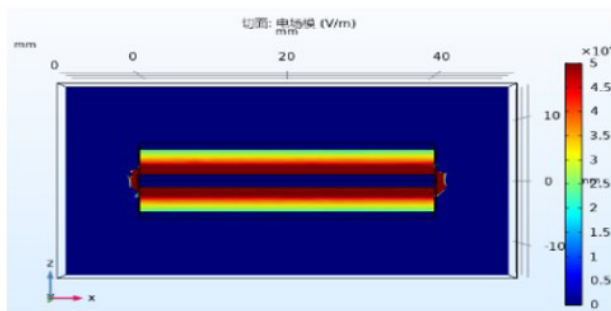
(b) electric potential of coaxial treatment chamber



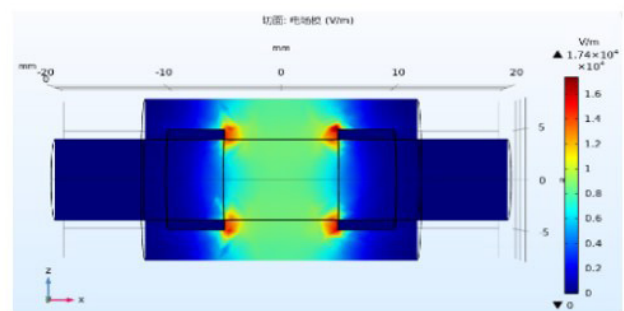
(c) electric potential of co-field treatment chamber



(d) electric field intensity of plate treatment



(e) electric field intensity of coaxial treatment chamber



(f) electric field intensity of co-field treatment chamber

Figure 4. The distribution of electric potential and electric field intensity in the cross section of various treatment chambers.

to a sharp increase in electric field intensity. It can be observed that there is an area of extremely high electric field intensity at the inner edge of the electrode in the co-field treatment chamber, that is, an electric field spike.

After that, additional experiments were carried out on the three treatment chamber structures, and it was found that the electric potential distribution and electric field intensity distribution did not change greatly in the process of increasing the electric field strength. This phenomenon proves that three treatment chamber, plate treatment chamber most uniform electric field, crushing capacity of each part, and coaxial treatment chamber and field chamber of the electric field distortion is serious, there is advantage process area--the advantage treatment for coaxial treatment chamber area near axis, realistically handle room work area is located in the channel between the two electrodes.

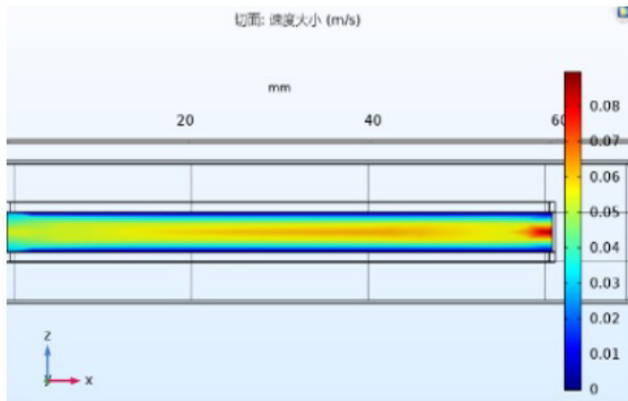
Flow field simulation results

The flow velocity distribution in each treatment chamber after stabilization is shown in Figure 5. The flow velocity in the plate treatment chamber is uniform (Figure 5a), and the highest flow velocity is ~ 88.6 mm/s. There is a large low-speed area around the cross section. The flow velocity distribution of

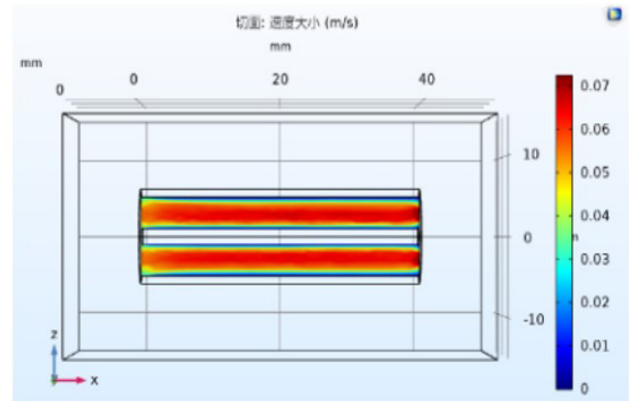
the coaxial treatment chamber (Figure 5b) is similar to that of the plate treatment chamber, with an average flow velocity of about 60 mm/s and a uniform distribution. A low flow velocity zone with a thickness of about 0.5 mm appears near the axis electrode and the inner wall. The flow field distribution in the co-field treatment chamber (Figure 5c) is similar to that in the coaxial treatment chamber without obvious low speed zone.

Temperature simulation results

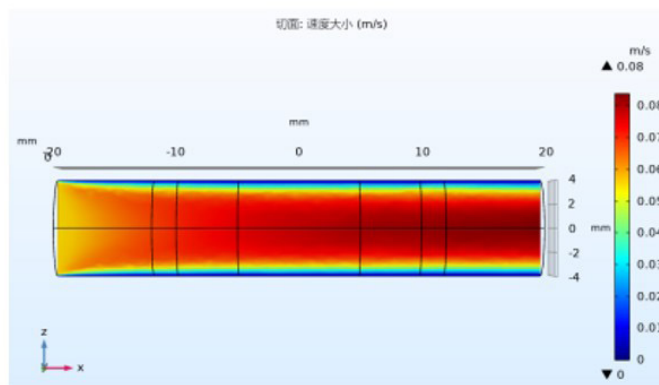
The cross section of the temperature field in various treatment chambers after 1s is shown in Figure 6. The temperature distribution in the plate treatment chamber (Figure 6a) after 1s is more balanced, about 325 K, and the temperature rise is 31.85 K, and the temperature rise rate at the entrance is lower than that at the exit. The temperature near the axis of the coaxial treatment chamber (Figure 6b) is significantly higher than that in other regions, about 383K(temperature rise rate 87.85 K/s), and gradually decreases outward. The temperature rise rate of the co-field treatment chamber (Figure 6c) is much lower than that of the other two treatment chambers, only 6.85 K at the junction between insulator and electrode inside.



(a) plate treatment chamber



(b) coaxial treatment chamber



(c) co-field treatment chamber

Figure 5. Cross section flow field distribution of various treatment chambers.

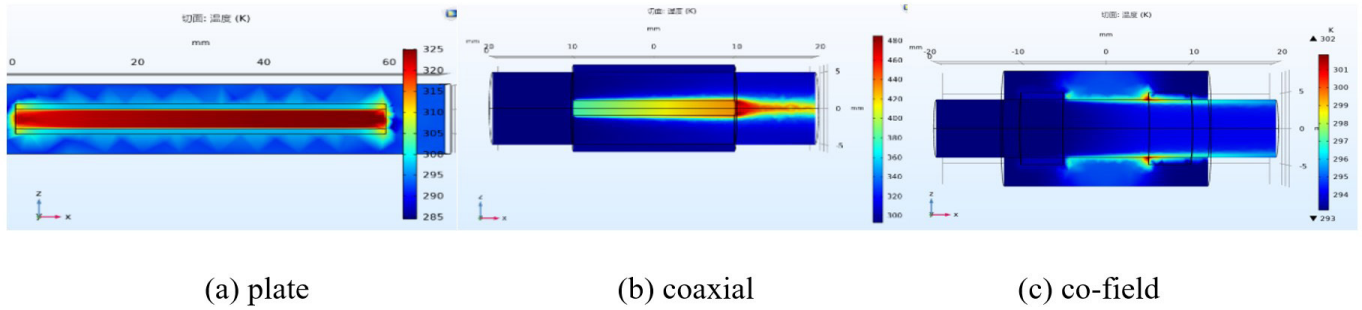


Figure 6. temperature field distribution in cross section of various treatment chambers.

4 Structural optimization design and simulation comparison of co-field treatment chamber

According to the above simulation, it can be found that there is a sharp electric field phenomenon on the inside of the electrode during the operation of the classical co-field treatment chamber, and there is a certain low-speed area behind the treatment area, and the effective treatment area is small. Aiming at these defects, a new structure of the co-field treatment chamber is designed in this study.

The structure of the co-field treatment chamber optimized in this study is shown in Figure 7. To eliminate the peak electric field, which is at the junction between the electrode and the insulator, the inner side of the electrode is rounded (radius 1 mm) in this design, and sets the fluid channel and an insulator interface to parabolic, to enhance the channel and electric field intensity, and increase the processing area velocity make its turbulence intensity increases, dead area to eliminate the flow velocity.

In this section, this study will use this design and other four commonly used fluid channel-insulator interface with different geometric shapes: embedded rectangle, embedded rounded rectangle (radius of rounded corner 3 mm), and embedded oval in the co-field treatment chamber to conduct a comparative simulation of electric field, flow field and temperature field coupling.

The electric field simulation results of each shape of the treatment chamber are shown in Figure 8. It can be seen in Figure 8a that the electric field intensity of the embedded rectangular processing area is improved to a certain extent compared with that of the classical structure without the embedded co-field treatment chamber, the electric field intensity of the effective processing area is increased to 8.99 kV/m. However, due to the extremely uneven connection, there is still a relatively obvious electric field with a peak of 18.6 V/m at the contact point between electrode and insulation material. The electric field intensity in the effective treatment area was further enhanced to 11.17 kV/m after the fillet of the embedded torque (Figure 8b), and the peak electric field was alleviated to a certain extent to 17.4 kV/m. The field intensity in the effective area of the embedded elliptical treatment chamber (Figure 8c) increases to 13.68 kV/m, and the peak field intensity decreases to 16.5 kV/m. In this design, the field intensity in the effective area is the largest among the four structures (Figure 8d), which

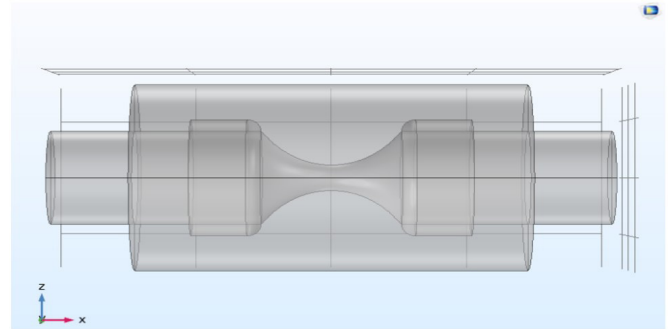
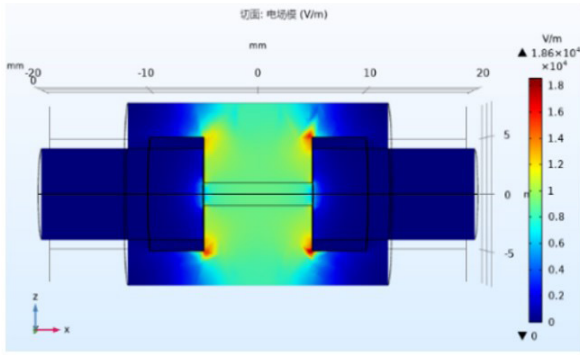


Figure 7. Parabolic co-field treatment chamber.

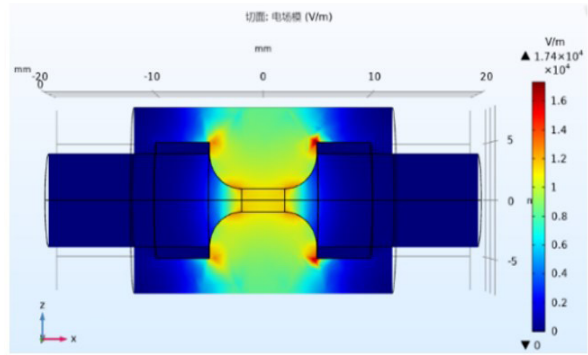
is 17.59 kV/m, and the peak electric field in the connection area between the inside of the electrode and the insulator is almost eliminated, and the maximum electric field intensity in this area is reduced to 13.15 kV/m.

Four structure along the treatment chamber temperature field simulation, as shown in the Figure 9 can be clearly observed nested rectangles (Figure 9a), embedded rounded rectangle (Figure 9b), embedded elliptic (Figure 9c) these three treatment chamber structure are inevitably in the fluid channel caused a wide range of temperature rising area, temperature rise within 1 s are reached more than 3 k, and the design (Figure 9d) temperature area is restricted within the fluid channel, Moreover, the temperature rise within 1s is only 0.93K, which greatly reduces the possibility of small bubbles in the suspension and reduces the loss during the operation of the treatment chamber.

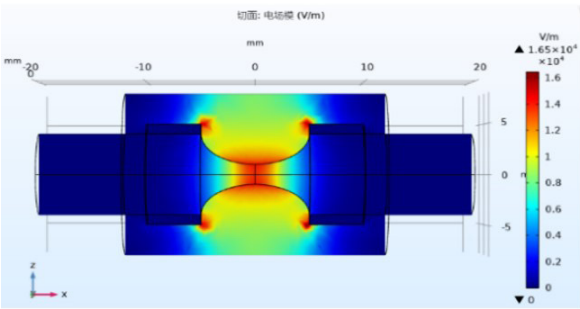
According to Table 2, the advantages of this design compared with other common structures can be seen directly: the electric field intensity of the treatment area is 20.03 kV/m, which is much higher than 8.29 kV/m of the classical co-field treatment chamber, and 112.80%, 79.32% and 46.42% of the other three optimized structures, respectively. The temperature rise within 1s is 0.93 K, which is 86.42% lower than that of the classical structure in the co-field treatment chamber, and about 2/3 lower than that of the other three structures. With the inner structure of the rounded electrode, the area where the spike electric field occurs is greatly reduced, and the intensity of the spike electric field is also reduced by 24.4% compared with the classical co-field treatment chamber structure.



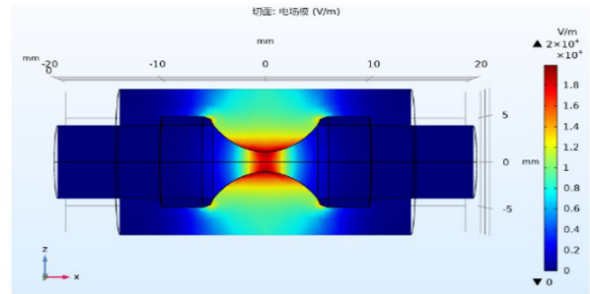
(a) the rectangle embedded



(b) rounded rectangle embedded

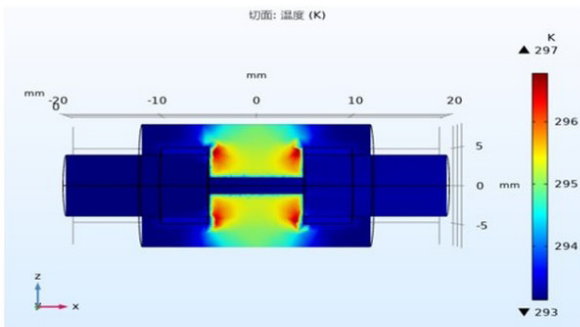


(c) oval shape embedded

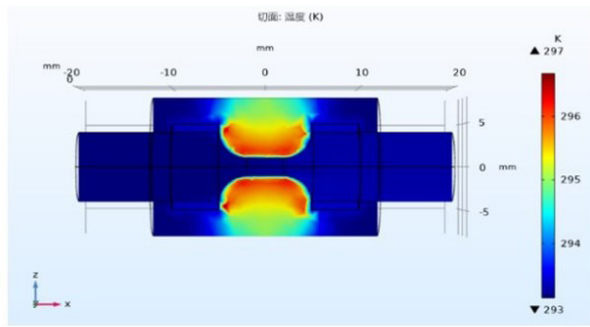


(d) our work

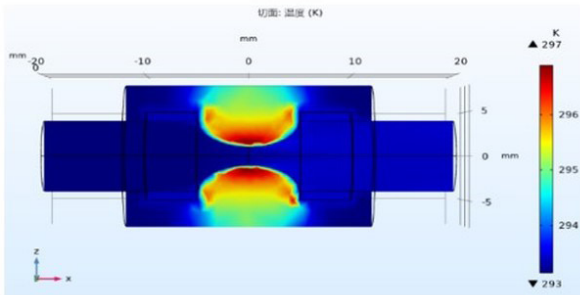
Figure 8. Electric field simulation results (electric field intensity distribution).



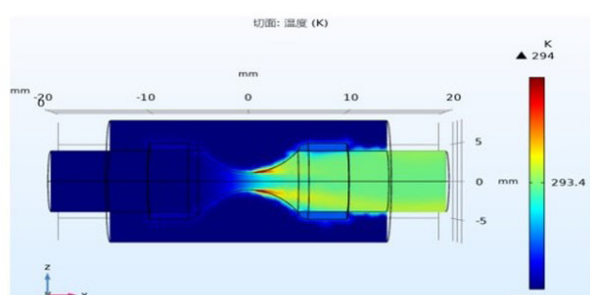
(a) the rectangle embedded



(b) rounded rectangle embedded



(c) oval shape embedded



(d) our work

Figure 9. Temperature simulation results.

Table 2. Comparison of simulation results.

Type of treatment chamber	Electric field intensity in the processing area (kV/m)	Velocity of the processing area (m/s)	Temperature rising (K/s)	Peak electric field intensity (kV/m)
Classic type	8.29	0.05	6.85	17.4
the rectangle embedded	8.99	1.27	3.35	18.6
rounded rectangle embedded	11.17	1.14	3.75	17.4
oval shape embedded	13.68	1.09	3.85	16.5
Ours	20.03	0.87	0.93	13.15

5 Conclusion

Using COMSOL Multiphysics, in this paper, the coupling simulation of electric field, flow field and temperature field of three kinds of high-voltage pulsed electric field treatment chambers (plate, coaxial and same field) used for cell lysis is carried out. The advantages and disadvantages of the three are analyzed respectively. It is found that there are obvious treatment areas in the co-field treatment chamber, and it is less affected by temperature rise effect.

In addition, aiming at the problems of low electric field intensity and severe sharp electric field in the classical structure of the co-field treatment chamber, this paper proposes a new structure of the co-field treatment chamber: the parabolic fluid channel shape with minimum inner diameter of 2 mm is used, and the inner side of the electrode is rounded (the radius of the rounded corner is 1 mm). Based on this design, this study established a three-dimensional model of parabolic same-field treatment chamber unit, and conducted simulation and comparative tests with COMSOL multi-physical field simulation software and the same-field treatment chamber of other three kinds of treatment chamber structures. It was found that this design has significant advantages in improving electric field intensity, eliminating electric field spikes, and reducing temperature rise. This will be conducive to the effective sterilization of food at the same time to ensure that its taste and nutritional value is not destroyed. It is expected that this study can provide a new idea for the structure optimization and design of the co-field treatment chamber used for food sterilization and food processing.

Funding

Natural Science Foundation of Hunan Province under Grant No:2021JJ31142.

References

- Abdilova, G., Terekhova, A., Shadrin, M., Burakovskaya, N., Fedoseeva, N., Artamonova, M., Ermienko, A., Smirnova, M., Grigoryants, I., & Strigulina, E. (2021). Study on the influence of different magnetic and electric field-assisted storage methods on non-thermal effects of food. *Food Science and Technology (Campinas)*, 42, e29921. <https://doi.org/10.1590/fst.29921>.
- Arshad, R. N., Abdul-Malek, Z., & Dastgheib, A. M. (2021a). Simulation study of coaxial treatment chambers for pef pasteurization: a critical review. *International Journal of Online & Biomedical Engineering*, 17(12), 93-107. <http://dx.doi.org/10.3991/ijoe.v17i12.25247>.
- Arshad, R. N., Abdul-Malek, Z., Roobab, U., Munir, M. A., Naderipour, A., Qureshi, M. I., El-Din Bekhit, A., Liu, Z.-W., & Aadil, R. M. (2021b). Pulsed electric field: a potential alternative towards a sustainable food processing. *Trends in Food Science & Technology*, 111, 43-54. <http://dx.doi.org/10.1016/j.tifs.2021.02.041>.
- Deng, H., Zhao, P. T., Yang, T. G., & Meng, Y. H. (2021). A comparative study of the cloudy apple juice sterilized by high-temperature short-time or high hydrostatic pressure processing: shelf-life, phytochemical and microbial view. *Food Science and Technology (Campinas)*, 42, e63620. <https://doi.org/10.1590/fst.63620>.
- Gentès, M. C., Caron, A., & Champagne, C. P. (2022). Potential applications of pulsed electric field in cheesemaking. *International Journal of Dairy Technology*, 75(2), 270-288. <http://dx.doi.org/10.1111/1471-0307.12854>.
- Glaser, R. W., Leikin, S. L., Chernomordik, L. V., Pastushenko, V. F., & Sokirko, A. I. (1988). Reversible electrical breakdown of lipid bilayers: formation and evolution of pores. *Biochimica et Biophysica Acta*, 940(2), 275-287. [http://dx.doi.org/10.1016/0005-2736\(88\)90202-7](http://dx.doi.org/10.1016/0005-2736(88)90202-7). PMID:2453213.
- Guo, F., Zhang, L., Liu, X., Peng, H. (2020). Micropore characteristics of spherical cells based on electroporation and pore size change equation. *Chinese Journal of Biomedical Engineering*, 39(05), 577-586.
- Lubicki, P., Cross, J. D., Jayaram, S., Mazurek, B., & Staroniewicz, Z. (1995). Inactivation of *Yersinia enterocolitica* Gram-negative bacteria using high-voltage pulse technique//IAS'95. In *Proceedings of the Conference Record of the 1995 IEEE Industry Applications Conference Thirtieth IAS Annual Meeting* (pp. 1338-1344). USA: IEEE.
- Naliyadhara, N., Kumar, A., Girisa, S., Daimary, U. D., Hegde, M., & Kunnumakkara, A. B. (2022). Pulsed electric field (PEF): avant-garde extraction escalation technology in food industry. *Trends in Food Science & Technology*, 122, 238-255. <http://dx.doi.org/10.1016/j.tifs.2022.02.019>.
- Prestes, A. A., Helm, C. V., Esmerino, E. A., Silva, R., & Prudencio, E. S. (2022). Conventional and alternative concentration processes in milk manufacturing: a comparative study on dairy properties. *Food Science and Technology (Campinas)*, 42, 42. <http://dx.doi.org/10.1590/fst.08822>.
- Qingxue, G. A. O., & Ping, X. (2017). Simulation analysis and optimization of high voltage pulsed electric field common field sterilization chamber. *Food and Machinery*, 33(8), 79-84.
- Rocha, C. S., Magnani, M., Ramos, G. L. P. A., Bezerril, F., Freitas, M. Q., Cruz, A. G., & Pimentel, T. C. (2022). Emerging technologies in food processing: impacts on sensory characteristics and consumer perception. *Current Opinion in Food Science*, 47, 100892. <http://dx.doi.org/10.1016/j.cofs.2022.100892>.
- Šalaševičius, A., Uždavinytė, D., Visockis, M., Ruzgys, P., & Šatkauskas, S. (2021). Effect of Pulsed Electric Field (PEF) on bacterial viability and whey protein in the processing of raw milk. *Applied Sciences*

- (Basel, Switzerland), 11(23), 11281. <http://dx.doi.org/10.3390/app112311281>.
- Sale, A., & Hamilton, W. (1967). Effects of high electric fields on microorganisms. I. Killing of bacteria and yeasts. *Biochimica et Biophysica Acta (BBA) - General Subjects*, 148(3), 781-788. [http://dx.doi.org/10.1016/0304-4165\(67\)90052-9](http://dx.doi.org/10.1016/0304-4165(67)90052-9).
- Sowmya, D., & Varadarajan, G. S. (2021). Anti-Cancerous effect of PEF treated Aloe barbadensis miller extract on MCF-7 Breast cancer cell lines. In *Proceedings of the 2021 IEEE 5th International Conference on Condition Assessment Techniques in Electrical Systems (CATCON)* (pp. 157-162). USA: IEEE.
- Tsong, T. Y. (1989). Electroporation of cell membranes. In E. Neumann, A. E. Sowers & C. A. Jordan (Eds.), *Electroporation and electrofusion in cell biology* (pp. 149-163). Boston, MA: Springer. https://doi.org/10.1007/978-1-4899-2528-2_9.
- Zeng, X., Yan, P., Cai, J., Zhang, Z., & Lin, S. (2021). Multi-physical field simulation and experiment of plate-type continuous treatment chamber. *Journal of South China University of Technology*, 2021, 49(3), 80-87.
- Xu, F., & Xiao, D. (2006). Model analysis and experimental study of pulsed electric field on cells. *High Voltage Engineering*, (06), 67-69+83. <http://dx.doi.org/10.13336/j.1003-6520.hve.2006.06.024>.
- Zand, E., Schottroff, F., Steinacker, E., Mae-Gano, J., Schoenher, C., Wimberger, T., Wassermann, K. J., & Jaeger, H. (2021). Advantages and limitations of various treatment chamber designs for reversible and irreversible electroporation in life sciences. *Bioelectrochemistry (Amsterdam, Netherlands)*, 141, 107841. <http://dx.doi.org/10.1016/j.bioelechem.2021.107841>. PMID:34098460.
- Zhang, Q., Barbosa-Cánovas, G. V., & Swanson, B. G. (1995). Engineering aspects of pulsed electric field pasteurization. *Journal of Food Engineering*, 25(2), 261-281. [http://dx.doi.org/10.1016/0260-8774\(94\)00030-D](http://dx.doi.org/10.1016/0260-8774(94)00030-D).
- Zhang, R., Fu, X., & Kou, M. (2016a). Effect of high voltage pulsed electric field on the crushing effect of Chlorella. *High Voltage Engineering*, 42(08), 2668-2674. <http://dx.doi.org/10.13336/j.1003-6520.hve.20160812039>.
- Zhang, S., Yan, W., & Gong, Q. (2016b). Multi-physical field simulation of high voltage pulsed electric field treatment chamber. *Packaging and Food Machinery*, 34(3), 38-41.
- Zhang, R., Xu, G., Wang, Y., & Fu, X. (2018). Study on membrane controlled electroporation under pulsed electric field. *High Voltage Engineering*, 44(7), 2254-2260. <http://dx.doi.org/10.13336/j.1003-6520.hve.20180628019>.